Flow-induced stresses and displacements in jointed concrete pipes, installed by pipe jacking method

Moses Karakouzian [1], Mehrdad Karami [2], Mohammad Nazari-Sharabian [3,*] and Sajjad Ahmad [4]

[1] Professor, Department of Civil and Environmental Engineering and Construction, University of Nevada Las Vegas, USA; mkar@unlv.nevada.edu

[2] M.Sc., Department of Civil Engineering, Isfahan University of Technology, Iran; karami.mehrdad.ce@gmail.com

[3] Ph.D. Candidate, Department of Civil and Environmental Engineering and Construction, University of Nevada Las Vegas, USA; nazarish@unlv.nevada.edu

[4] Professor, Department of Civil and Environmental Engineering and Construction, University of Nevada Las Vegas, USA Affiliation 2; sajjad.ahmad@unlv.edu

* Correspondence: nazarish@unlv.nevada.edu

Abstract: Transient flows result in unbalanced forces and high pressure in pipelines. Under these conditions, the combined effects of flow-induced forces along with sudden pipe displacements can create cracks in the pipeline, especially at the junctions. This situation consequently results in water leakage and reduced operational efficiency of the pipeline. In this study, displacements and stresses in a buried pressurized water transmission pipe installed by pipe jacking method are investigated using numerical modeling and considering interactions between fluid, pipe, and soil. The analyses were performed consecutively under no-flow, steady flow, and transient flow conditions, in order to investigate the effects of flow conditions on displacements and stresses in the system. Analyses of the results show that displacements and stresses in the jointed concrete pipes are significant under transient flow conditions. Moreover, because of pressure transient effects, maximum tensile stresses exceed the tensile strength of concrete at the junctions, leading to cracks and consequent water leakage.

Keywords: Fluid-Structure Interaction, Soil-Structure Interaction, Transient Flow, Pipe Jacking, Numerical Modeling, Abaqus FEA

1. Introduction

Pipe failures are usually a complex function of different circumstances, including pipe properties, internal and external loadings, and environmental factors. Generally, when applied forces exceed the bearing capacity of the pipe materials, failure occurs [1]. Among pipe damage and causes, several failures have been reported due to pressure transient effects [2,3,4]. Transient pressure in pipe networks is generally formed due to factors such as sudden changes in valve operations, starting or stopping of pumps, the sudden change in reservoir level, and changes in the demand conditions. In such cases, the kinetic energy of the fluid is reduced significantly, and pressure waves are transmitted along the pipeline. This high-pressure build-up can damage the pipeline by creating sudden pipe displacements and excessive stresses in the pipe wall [5]. Figure 1 and 2 show stress distribution in a pressurized pipe, and stresses acting on the pipe wall.
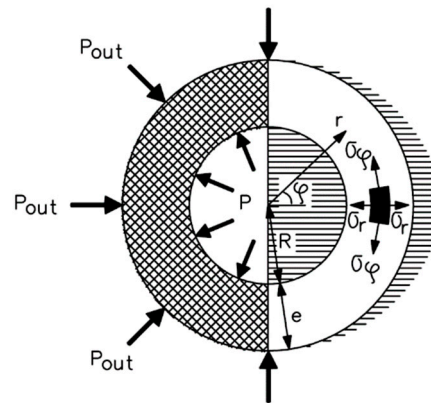
43
44   **Figure 1.** Stress distribution in a pressurized pipe [5]

45
46   (a)   (b)
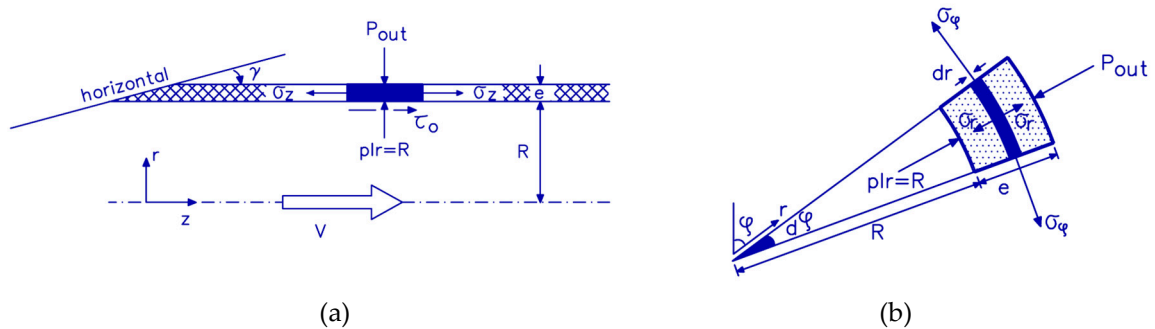
47   **Figure 2.** a) Side view (z–r plane): stresses acting on pipe wall
48   b) Cross-sectional view (r–φ plane): normal stresses acting on an element of pipe wall [5]

49   In Figure 1, P_{out} is the soil overburden pressure on the pipe, P is the transient pressure of the
50 fluid, R is the internal radius, and e is the thickness of the pipe.

51   According to Figure 2, by considering the existence of two-dimensional axially symmetric
52 stresses in a circular ring subjected to the internal pressure P and external pressure P_{out} (soil pressure),
53 the pipe displacements can be described by Equation 1 and 2, as:

$$\rho_t \frac{\partial \dot{u}_z}{\partial t} = \frac{\partial \sigma_z}{\partial z} \tag{1}$$

$$\rho_t \frac{\partial \dot{u}_r}{\partial t} = \frac{1}{r}\frac{\partial (r\sigma_r)}{\partial r} - \frac{\sigma_\varphi}{r} \tag{2}$$

54 By solving Equation 1 and 2, the hoop and radial stresses can be calculated using Equation 3 and 4,
55 as:

$$\sigma_\varphi = -\frac{A}{r^2} + 2C \tag{3}$$

$$\sigma_r = \frac{A}{r^2} + 2C \tag{4}$$

56 A and C are determined by satisfying the following boundary conditions:

$$\sigma_r \big|_{r=R} = -P(z,t) \tag{5}$$

$$\sigma_r \big|_{r=R+e} = -P_{out} \tag{6}$$

57   It follows that:

$$A = \frac{R^2(R+e)^2(P_{out}-P)}{2(R+0.5e)e} \tag{7}$$

$$C = \frac{R^2P-(R+e)^2P_{out}}{4(R+0.5e)e} \tag{8}$$

58   Finally, the averaged values of σ_φ and σ_r are presented in Equation 9 and 10, as:

$$\bar{\sigma}_\varphi = \frac{1}{e}\int_R^{R+e}\sigma_\varphi dr = \frac{R}{e}P - \frac{R+e}{e}P_{out} \tag{9}$$

$$\bar{\sigma}_r = \frac{1}{2\pi(R+0.5e)e}\int_R^{R+e}2\pi r\sigma_r dr = -\frac{3}{4}P - \frac{1}{4}P_{out} \tag{10}$$

59   In recent years, the use of underground structures such as pressurized water pipes for the
60 distribution of water has increased. Trenched and trenchless drilling are two methods commonly
61 used for the construction of buried pipelines [6]. In the trenched method, the soil is removed to form
62 a trench in the ground, and as the pipes are installed, the trench is filled with soil again. In this
63 method, issues such as reduced enclosing tensions around the pipe, due to lack of proper soil
64 compaction can occur, which can consequently result in inadequate safety and instability of the
65 structure, in the event of pressure transient conditions and pipe displacements [1]. Whereas in
66 trenchless drilling, soil compaction and stresses within the soil are not significantly affected. Pipe
67 jacking is a trenchless drilling technique, used for the installation of underground structures such as
68 pipelines, ducts, and culverts. In this method, powerful hydraulic jacks are used to push concrete or
69 steel pipes through the ground at the same time as drilling is taking place within the shield [7]. In
70 this method, the end connection of a fitting that is to be assembled into another fitting is called "the
71 spigot", and the female connection of the pipe fitting is referred to as "the socket". The spigot end of
72 a fitting is inserted into the socket. Spigot and socket joint pipes are joined and sealed using a rubber
73 ring (Figure 3).

74
75   **Figure 3.** The spigot and socket ends of a concrete pipe in pipe jacking method [8]

76   *1.1. Literature Review and Motivation*

77   Kyriakides and Babcock [9] studied the propagation of internal pressures in circular pipes. They
78 concluded that transient pressures cause significant stresses in the pipes. In another effort, Milligan
79 et al. [10] investigated the pipe-soil interactions in the pipe jacking method and proposed a theoretical
80 model for the interactions. Using numerical modeling, Valiente [11] evaluated failures in concrete
81 pipes due to internal pressures. He presented equations to estimate maximum stresses in the pipe.
82 Gysling [12] conducted an experimental study on vibrations and displacements around unburied

83 pipes due to dynamic flows. He used sensors to measure displacements, and concluded that unsteady
84 pressures could be damaging to the pipeline.

85   Wasmer et al. [13] investigated the crack growth in straight and bent unburied cast iron pipes
86 under steady internal pressures, and proposed an analytical model. Meis et al. [14] conducted a
87 research study to determine the static and dynamic behavior of some typical restrained and
88 unrestrained underground pipe joints due to internal pressure and earthquakes. Gou [15] studied a
89 pipeline under oblique loading. He demonstrated the effect of pipe burial depth on displacements
90 around the pipe. Schmitt et al. [16] investigated pipeline failure due to dynamic pressure effects in a
91 case study in Tunisia. They used numerical modeling to investigate damages in the pipe. Tijsseling
92 [5] investigated the impact of dynamic pressures in a pressurized pipe, considering fluid-structure
93 interactions. He presented equations for determining tensions and displacements in unburied pipes.
94 Using the finite element method, Lydell and Riznic [17] conducted a survey on the damages to pipes
95 in various projects. They categorized various factors, including internal pressures in the pipe.

96   More recently, Vazouras et al. [18] investigated the mechanical behavior of buried steel pipelines
97 crossing an active strike-slip fault. They studied the effects of fault displacements and evaluated the
98 critical strain in the pipeline. Wu et al. [19] used a three-dimensional finite element analysis to study
99 the effects of load and displacement-controlled bending on the plastic collapse of pressurized pipes.
100 Rezai et al. [1] studied the impact of transient hydraulic conditions on pipe failures by analyzing
101 historical records and investigating different case studies. Wang [20] used the finite element method
102 to study damages in underground pipes as a function of soil overburden and surface loads. He
103 proposed a method to evaluate the magnitude of damage in pipes within a short period of time as a
104 result of an impact load on the surface. Xu et al. [21] studied the effects of soil overburden and traffic
105 loads on a concrete pipeline. The results indicated that applied loads had considerable impacts on
106 damages to the pipe.

107   The literature review indicates that flow-induced stresses and displacements in buried
108 pressurized water transmission pipes installed using trenchless drilling (pipe jacking method) have
109 not been investigated. Therefore, this study aims to fill this gap in the literature.

2. Materials and Methods

111   In this research, a typical water transmission concrete pipe in a soil environment is numerically
112 studied using the Abaqus FEA (Finite Element Analysis) under three scenarios: a) drilling and pipe
113 installation (no-flow condition); b) steady flow in the pipe; c) transient flow in the pipe. General steps
114 for setting up the model are presented in the following sub-sections.

2.1. Model Geometry

116   Geometries of the soil mass, pipe cross-section, and model boundaries are shown in Figure 4. A
117 long concrete pipe, with internal and external radii of 45 and 50 cm, respectively, was modeled.
118 Model boundaries were determined by trial and error in a way that they show the least impact on
119 analysis results.
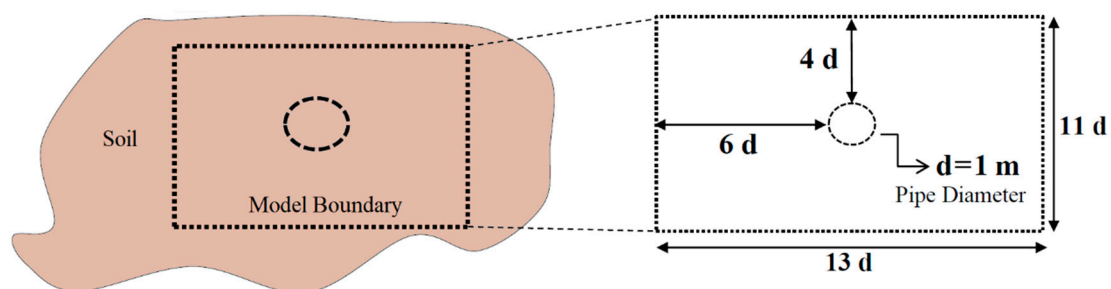
120
121   **Figure 4.** Cross section of the pipe and soil

122   *2.2. Soil and Material Properties*

123   The geomechanical properties of the soil mass were selected based on the characteristics of
124   normally consolidated clay in urban areas [22]. Moreover, the properties of the pipe were selected
125   based on the characteristics of typical water transmission concrete pipes [23]. Table 1 presents soil
126   and material properties used in the model.

127   **Table 1.** Properties of the materials used in the model [22, 23]

Material	Parameter	Value
Soil	Log. of Bulk Modulus	0.026
	Poisson's Ratio	0.4
	Tensile Limit	0
	The angle of Internal Friction	23
	Log. of Plastic Bulk Modulus	0.174
	Density (Kg/m³)	1800
	Stress Ratio	0.94
	Initial Yield Surface Size (Pa)	4884
	Wet Yield Surface Size	1
	Flow Stress Ratio	0.778
Concrete	Young's Modulus (GPa)	20
	Compressive Strength (MPa)	28.3
	Tensile Strength (MPa)	3
	Poisson's Ratio	0.25
	Density (Kg/m³)	2500
Water	Density (kg/m³)	1000
	Bulk Modulus (GPa)	2.7

128   *2.3. Flow Characteristics*

129   Internal pressure and flow velocity in the pipe under steady flow condition were selected to be
130   0.5 MPa (72.52 psi) and 4 m/s, respectively, as typical values in urban water transmission pipes.

131   *2.4. Modeling Procedure*

132   In the present study, the general assumptions that were necessary to model the FSI (fluid-
133   structure interaction) problem are as follows:
134   • The surrounding soil is monolith.
135   • The concrete lining behavior is considered as non-linear.
136   • A damage plasticity behavior is considered in the concrete lining.
137   • The CPE8R (8-node plane strain quadrilateral, biquadratic displacement, reduced integration)
138   elements are used for the simulation of the concrete pipe.
139   • Based on the Cam-Clay criterion, the soil is considered as a plastic material.
140   • Dynamic explicit method is applied to solve the finite element equations in the Abaqus FEA.

141   2.4.1. Acoustic Environment

142   Inside a pressurized water pipe, the only degree of freedom in nodes of the finite element model
143   of the fluid is pressure. In Abaqus FEA, acoustic environments and acoustic materials possess this
144   feature. An acoustic environment is an elastic environment where no shear stress is present
145   (assuming non-viscous fluid), and the pressure is proportional to volumetric strain. Acoustic
146   environments consider the effects of inertia and fluid compressibility. Pressure wave propagation
147   can also be simulated in these environments [24]. Therefore, in this study, acoustic elements were

148 implemented to simulate fluid motion in the pipe, in order to investigate the impact of transient
149 pressures on pipe displacements and the distribution of stresses in the pipe wall.

150 2.4.2. Interactions Between Model Components and Meshing

151   As stated above, the only variable in the acoustic environment is pressure. The value of this
152 variable was applied to each node by applying initial conditions using a quasi-static wave method
153 [25]. The interactions between the pipe and fluid were introduced to the model by coupling
154 displacement matrixes of the inner pipe surface with displacement matrixes of the fluid boundary
155 elements. Moreover, the interactions between the pipe and soil were introduced to the model by
156 defining cohesive elements between the soil and the outer pipe surface. Figure 5 shows the meshing
157 of the soil, pipe, and fluid environments in a 3D view.
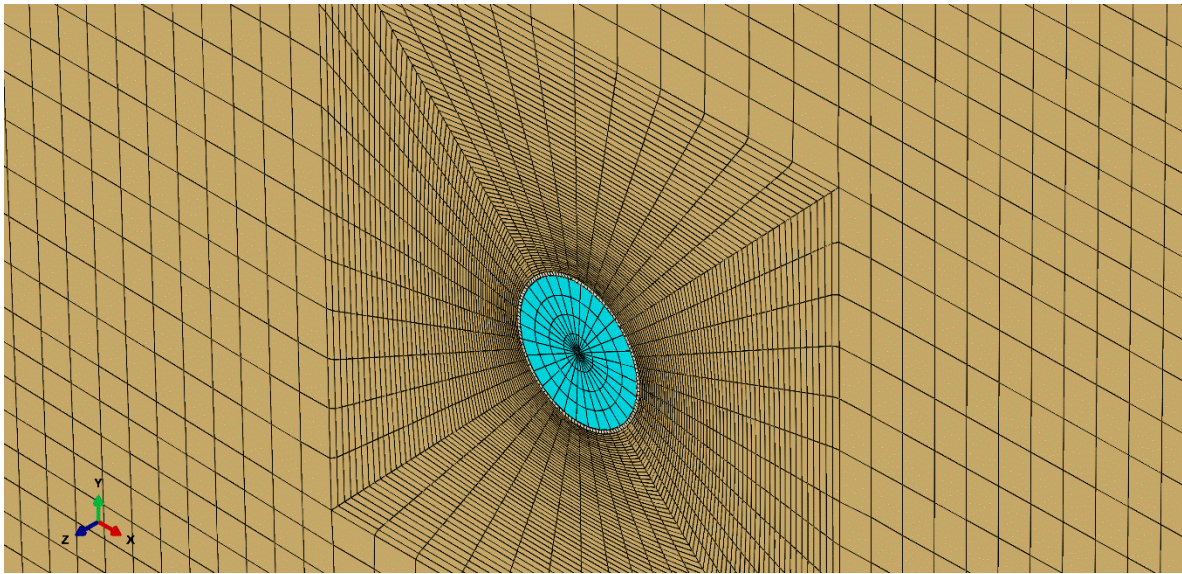
158
159   **Figure 5.** Finite element model mesh – 3D View

160 2.4.3. Transient Flow in The Pipe

161   To create transient flow in the pipe, it was assumed that 90% of a valve on the path was closed.
162 In this condition, based on hydraulic analysis using the method of characteristics (MOC) [26], flow
163 velocity upstream of the valve will reach 1 m/s, and pressure waves will form in the pipe. Figure 6
164 shows the change in flow velocity as a result of the relative valve closure percentage and the closure
165 time. The flat lines in the figure continue until the end of the simulation time.
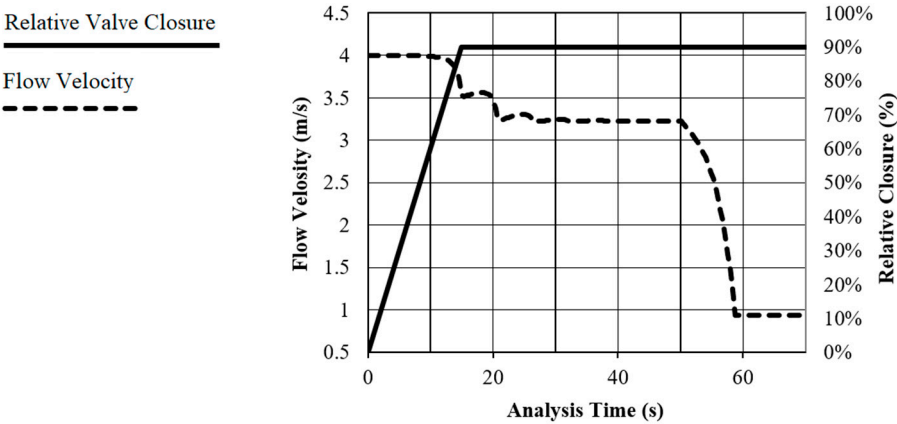
166
167   **Figure 6.** Flow velocity upstream of the valve and relative valve closure

168   If the time it takes to close the valve is less than wave travel time, the change in pressure head
169   can be obtained using Equation 11 [27]. According to Figure 6, the time it takes to close 90% of the
170   valve is about 15 s, while the wave travel time is about 59 s. Therefore, Equation 11 is applicable.

$$\Delta H = \frac{a}{g} \Delta V \tag{11}$$

$$a = \sqrt{\frac{1}{\rho_w (\frac{1}{k_w} + \frac{d}{E.e})}} \tag{12}$$

171   In Equation 11, ΔH (m) is the change in pressure head, a (m/s) is the pressure wave velocity, g is
172   the acceleration of gravity, and ΔV (m/s) is the change in water velocity in the pipe. In Equation 12,
173   ρ_w (kg/m³) is the specific mass of water, k_w (GPa) is the bulk modulus of water, d (m) is the pipe
174   diameter, E (GPa) is the modulus of elasticity of concrete, and e (m) is the thickness of the pipe [28].
175   The calculated values for a and maximum pressure under the transient flow condition are presented
176   in Table 2.

177

Table 2. Transient flow characteristics

Parameter	Value
a (m/s)	854
Max. Pressure (MPa)	2.61 (378.55 psi)

178   The calculated maximum transient pressure was applied to fluid elements in the model as
179   impact load. The transient pressure from fluid elements transfers to pipe elements, leading to pipe
180   displacements and stresses in the pipe wall.

181   **3. Results**

182   In the following sections, displacements in the soil environment and stresses in the pipe wall are
183   presented. Displacements under all scenarios are measured relative to their position right after
184   drilling and pipe installation (before reaching a new equilibrium). The location where displacements
185   and stresses are analyzed is near the valve, and the displacements in each stage are cumulative.

186   *3.1. No-Flow Condition*

187   Figure 7 and 8 show vertical (U_2) and horizontal (U_1) displacements in the soil environment,
188   respectively, and Figure 9 shows stresses in the pipe wall under no-flow condition. In Figure 9, as
189   well as in other figures showing stress distribution contours in the following sections, the blue color
190   shows areas in compression, while red shows areas in tension.

191
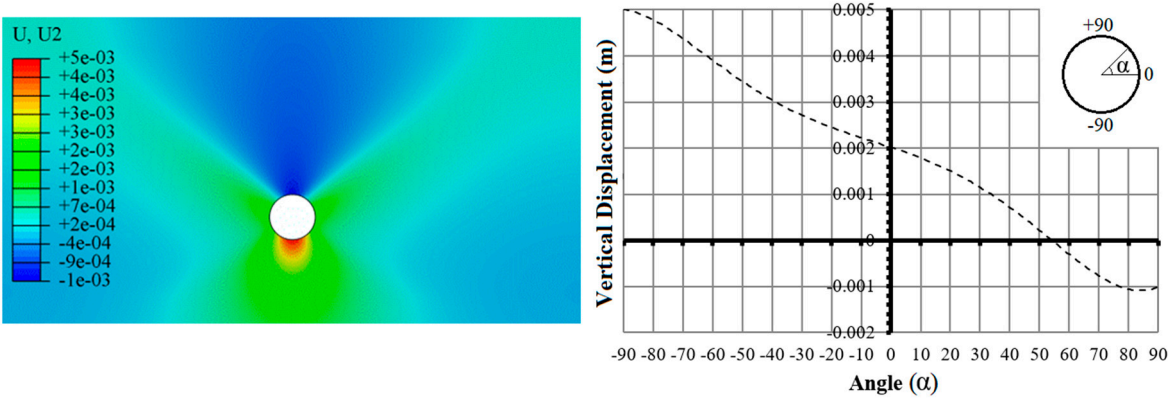
192   **Figure 7.** Displacements in the vertical direction under the no-flow condition
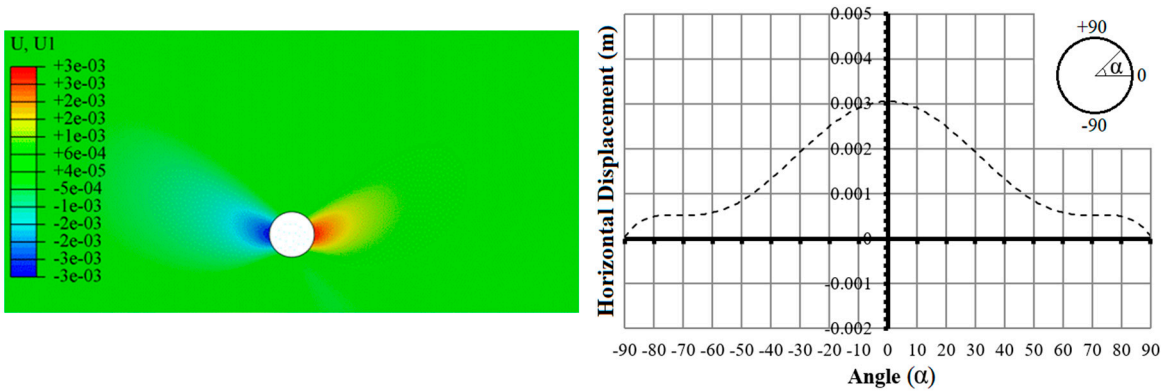
194   **Figure 8.** Displacements in the horizontal direction under the no-flow condition
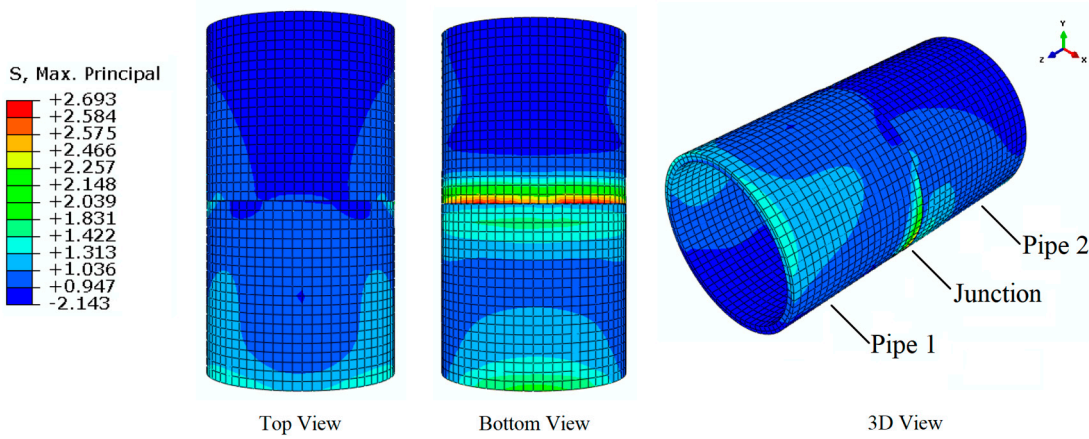
196   **Figure 9.** Stresses in the pipe wall under no-flow condition (MPa)

197   After drilling and pipe installation, distribution of stresses in the soil will change, and
198   eventually, due to the stress release phenomenon, the soil mass will reach a new equilibrium. Figure
199   7 shows that soil at the bottom of the section has become swollen. The amount of this uplift at the
200   bottom (5 mm) is greater than the amount of displacement in the crown (1 mm). According to Figure
201   8, horizontal displacements on the top and bottom sides are quite symmetrical and uniform, with a
202   maximum of 3 mm on the sides. Therefore, under the no-flow condition and due to unloading and
203   inflation of the soil, among all displacements, the greatest occurs at the bottom.

204   Stress distribution contours mostly show compression (blue) at the top and tension (red) at the
205   bottom of the pipe (Figure 9). Under this condition, the highest tensions occurred at the bottom of the
206   pipe with a maximum value of 2.69 MPa (390.15 psi) at the junction.

207   *3.2. Steady Flow Condition*

208   Figure 10 and 11 show vertical (U2) and horizontal (U1) displacements in the soil environment,
209   respectively, and Figure 12 shows the stresses in the pipe wall under steady flow condition.
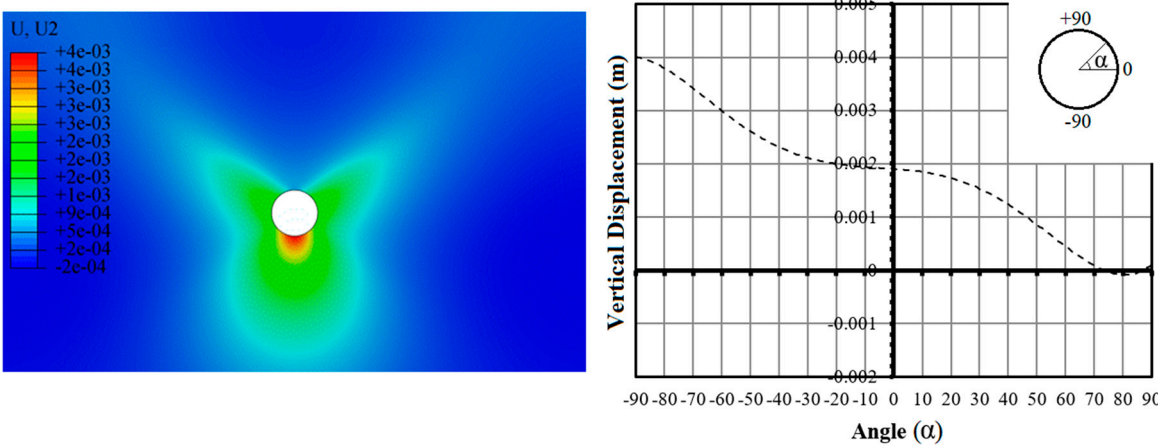
Figure 10. Displacements in the vertical direction under steady flow condition
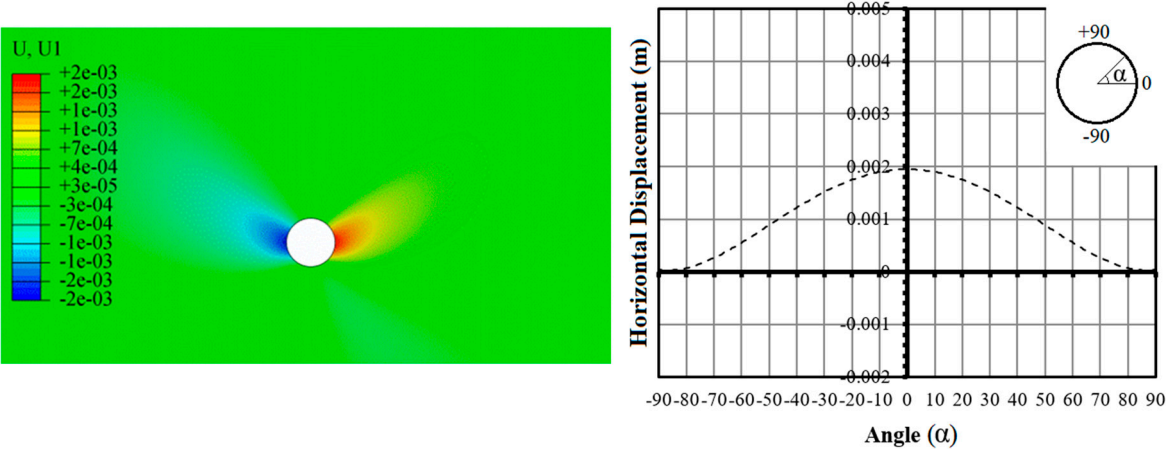
Figure 11. Displacements in the horizontal direction under steady flow condition
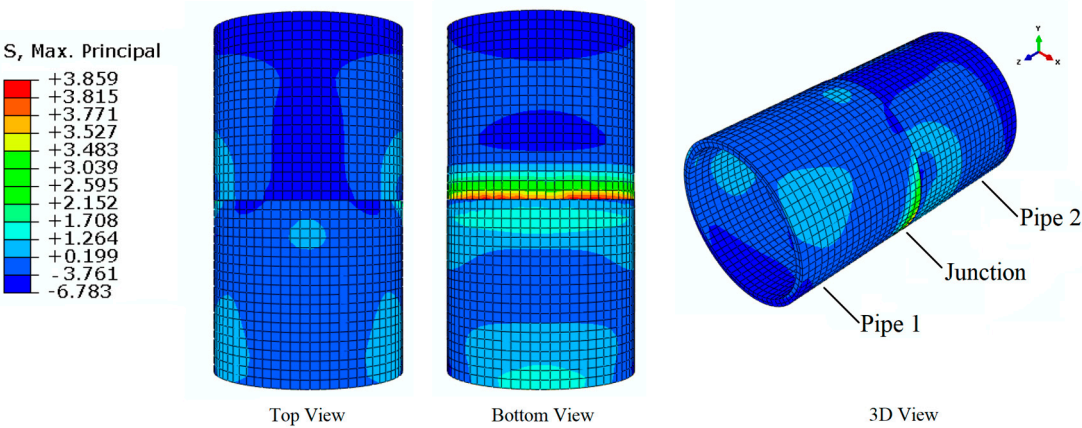
Figure 12. Stresses in the pipe wall under steady flow condition (MPa)

As mentioned earlier, in this scenario, the pressurized pipe is operating under a steady flow with 0.5 MPa (72.52 psi) of pressure. Due to this pressure, as well as the fluid weight, the concrete pipe moves, and this displacement transfers to the surrounding soil. As a result, displacements that took place under no-flow condition will change. The figures show that the maximum displacement under the steady flow condition is 1 mm, both in vertical and horizontal directions. This value is obtained from the maximum vertical pipe displacement difference in Figure 7 and 10. The same value is obtained by comparing horizontal displacements in Figure 8 and 11.

Similar to the no-flow condition, stress distribution contours mostly show compression at the top, and tension at the bottom of the pipe (Figure 12). Under this condition, due to the addition of the

225　internal pressure, the highest tensions occurred at the bottom of the pipe, with a maximum value of
226　3.86 MPa (559.85 psi) at the junction.

227　*3.3. Transient Flow Condition*

228　　　Figure 13 and 14 show vertical (U_2) and horizontal (U_1) displacements in the soil environment,
229　respectively, and Figure 15 shows the stresses in the pipe wall under transient flow condition.

230
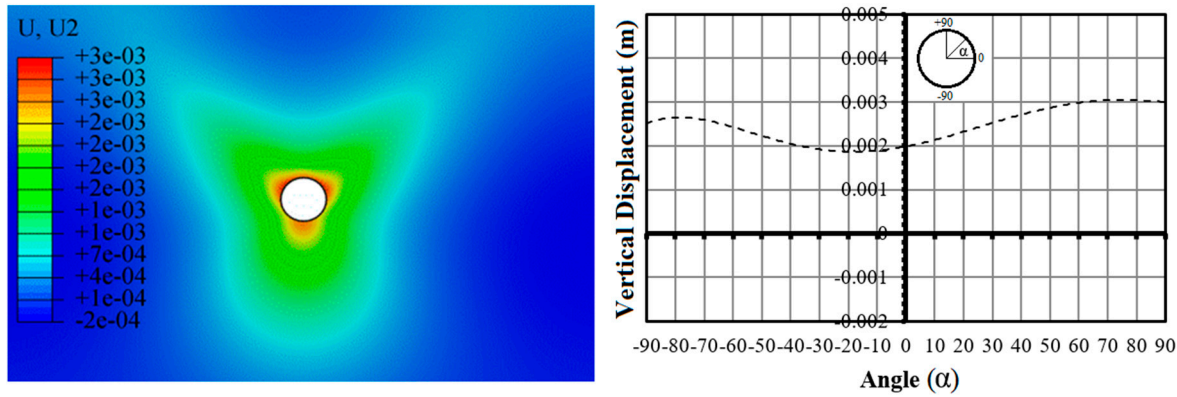
231　　　　　　**Figure 13.** Displacements in the vertical direction under transient flow condition

232
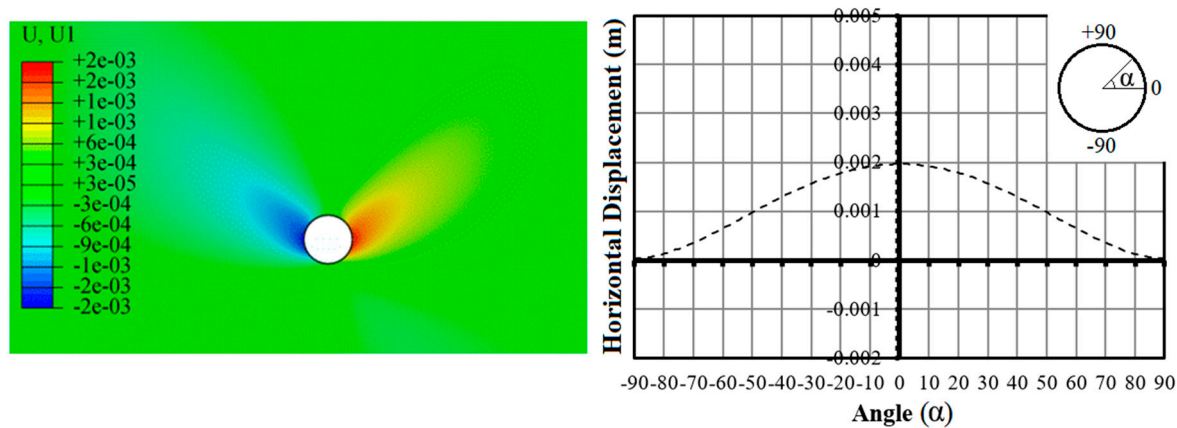
233　　　　　　**Figure 14.** Displacements in the horizontal direction under transient flow condition

234
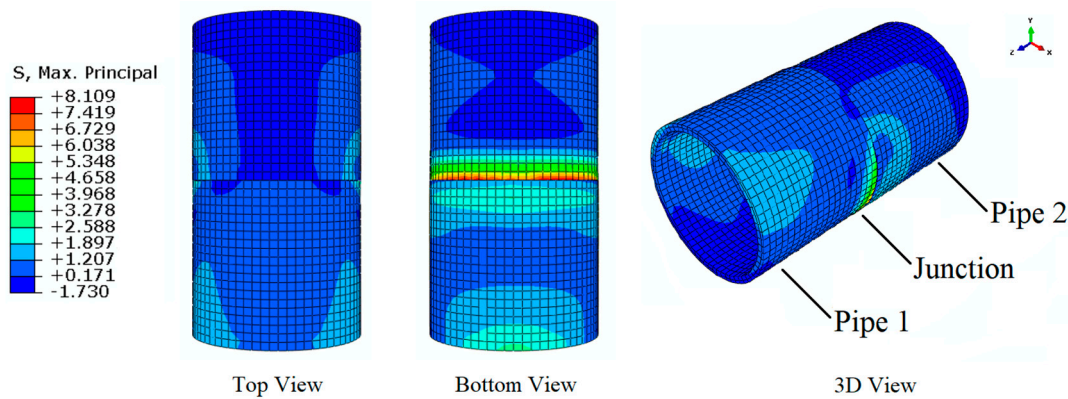
235　　　　　**Figure 15.** Stresses in the pipe wall under transient flow condition (MPa)

236　　　According to Figure 13 and 14, relative to steady flow condition, displacements in the soil have
237　increased under the influence of transient pressures in the pipe. The results obtained at this stage
238　indicate that maximum displacements occurred at the upper portions of the section, with a maximum
239　value of 3.1 mm in the crown.

240   Similar to the two previous conditions, stress contours show areas under compression at the top
241   and areas under tension at the bottom of the pipe. In the event of a transient flow, the maximum
242   tension remained at the bottom of the pipe, with a maximum value of 8.1 MPa (1174.81 psi) at the
243   junction.

4. Discussion

245   In Figure 16, the absolute value of total displacements (resultant of vertical and horizontal
246   displacements) under each scenario are shown. $U_{No-flow}$, U_{Steady}, and $U_{Transient}$, refer to total displacements
247   under no-flow, steady flow, and transient flow conditions, respectively.
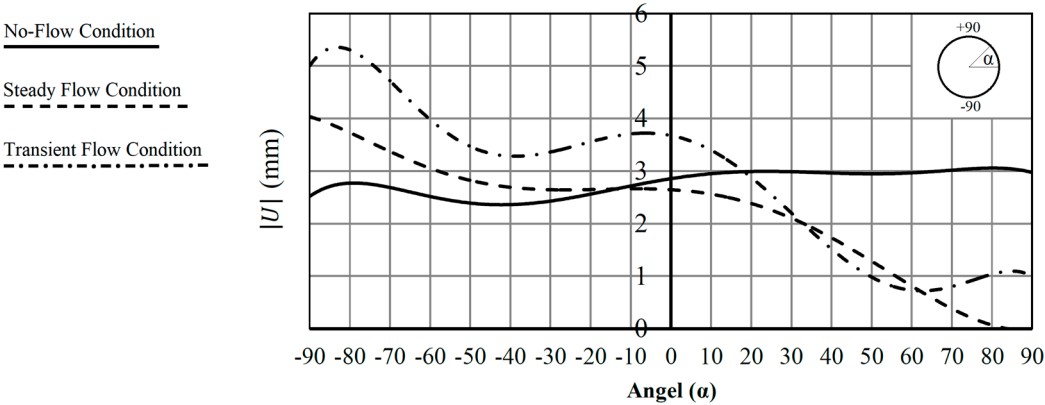
248
249   **Figure 16.** Total displacements under: no-flow, steady flow, and transient flow conditions

250   Figure 16 shows that under the no-flow condition, maximum displacements occurred at the
251   bottom of the section, which can be attributed to soil inflation, as a result of unloading the soil, soil
252   overburden, soil type, and distribution of loads in the drilled environment. Under steady flow
253   condition, the greatest displacement occurred at the bottom of the section, which can be attributed to
254   the internal pressure, fluid weight, and soil overburden. Finally, under transient flow condition, the
255   entire section of the pipe moved upward, and the maximum displacement occurred in the crown.
256   Concerning stresses, junctions were the most critical points. In all cases, the maximum compressive
257   and tensile stresses were formed at the junction.

258   Table 3 summarizes the maximum displacements along with the maximum compressive and
259   tensile stresses in the pipe wall under each scenario.

260   **Table 3.** Maximum displacements and stresses under each scenario

Scenario	Max. Displacements (mm)		Max. Stresses (MPa)	
	Vertical	Horizontal	Tensile	Compressive
No-flow condition	5	3	2.69 (390.15 psi)	2.14 (310.38 psi)
Steady flow	1	1	3.86 (559.85 psi)	6.78 (983.36 psi)
Transient flow	4	1	8.11 (1174.81 psi)	1.73 (250.92 psi)

261   Considering the range of 2.2 to 4.2 MPa for the tensile strength of concrete, under transient flow
262   condition, the tensile stress in the concrete pipe wall exceeds this range. High tensile stresses will
263   cause cracks in the pipe wall, especially at the junctions, and consequently result in water leakage,
264   soil wash, and generally reduced operational capacity of the pipeline.

5. Conclusions

266   A concrete water transmission pipe installed underground in ordinary compacted clay soil using
267   trenchless drilling (pipe jacking method) was modeled in Abaqus FEA. The purpose of this study
268   was to investigate flow-induced stresses in the pipe wall and displacements in the soil environment,
269   under no-flow, steady flow, and transient flow conditions in the pipe. The following are the key
270   findings of this study:

- Under the no-flow condition, the most significant displacements occurred at the bottom of the section. This can be attributed to the soil inflation phenomenon, as a result of drilling and alteration of stress distribution in the soil environment.
- Under steady flow condition, the soil environment showed small displacements, due to the internal pressure and fluid weight in the pipe.
- By the occurrence of transient pressure due to the event of transient flow in the pipe, the displaced region was enlarged, and the pipe and surrounding soil showed an upward movement.
- Under all scenarios, maximum compressive and tensile stresses were formed at the junction. The maximum value was observed under the transient flow condition, where the tensile stress exceeded the allowable tensile capacity of the concrete. This situation will cause cracks in the pipe wall and consequently leads to water leakage and reduced operational capacity of the pipeline.

Future work can be done on optimizing the valve closure pattern, considering the internal pressure in the pipe, existing soil overburden on the pipe, and soil type, in order to minimize transient pressures and resultant pipe displacements. Moreover, a comprehensive parametric study can be performed on different model components to investigate the impact of each parameter on the model results.

Author Contributions: conceptualization, Mehrdad Karami; methodology, Moses Karakouzian, Mehrdad Karami, Mohammad Nazari-Sharabian, Sajjad Ahmad; software, Mehrdad Karami; writing—original draft preparation, Mehrdad Karami and Mohammad Nazari-Sharabian; writing—review and editing, Moses Karakouzian and Sajjad Ahmad.

Funding: This research received no external funding

Conflicts of Interest: The authors declare no conflict of interest.

References

1. Rezaei, H.; Ryan, B.; Stoianov, I. Pipe failure analysis and impact of dynamic hydraulic conditions in water supply networks. *Procedia Eng.*, **2015**, 119, 253-262.
2. Kodikara, J.; Rathnayaka, S.; Zhang, J.; Crawly, C.; Zhang, D.; Blaha, F. Lessons Learned from Large-Diameter Pipe Failure Case Studies. *Pipelines*, 2017, doi:10.1061/9780784480885.052
3. Zarghamee, M. S.; Ojdrovic, R. P. Some Lessons Learned from Failure of a Pipeline. *Pipelines*, **2006**, doi:10.1061/40854(211)37
4. Schmitt, C.; Pluvinage, G.; Hadj-Taieb, E.; Akid, R. Water pipeline failure due to water hammer effects. *Fatigue Frac. Eng. Mater. Struct.*, **2006**, *29*(12), 1075-1082, doi:10.1111/j.1460-2695.2006.01071.x
5. Schmitt, C.; Pluvinage, G.; Hadj-Taieb, E.; Akid, R. Water pipeline failure due to water hammer effects. *Fatigue Frac. Eng. Mater. Struct.*, **2006**, 29(12), 1075-1082, doi:10.1111/j.1460-2695.2006.01071.x
6. Ma, B.; Najafi, M. Development and applications of trenchless technology in China. *Tunnelling Underground Space Technol.*, **2008**, 23(4), 476-480.
7. Yen, J.; Shou, K. Numerical simulation for the estimation the jacking force of pipe jacking. *Tunnelling Underground Space Technol.*, **2015**, 49, 218-229.
8. Langley Concrete - Precast concrete products. Available online: http://www.langleyconcretegroup.com (accessed 09 Oct. 2019).
9. Kyriakides, S.; Babcock, C. D. Experimental determination of the propagation pressure of circular pipes. *J. Pressure Vessel Technol.*, **1981**, 103(4), 328-336.
10. Milligan, G. W. E.; Norris, P, Pipe–soil interaction during pipe jacking. *Proc. Inst. Civ. Eng. Geotech. Eng.*, **1999**, 137(1), 27-44.
11. Valiente, A. Stress corrosion failure of large diameter pressure pipelines of prestressed concrete. *Eng. Fail. Anal.*, **2001**, 8(3), 245-261.
12. Gysling, D. L. U.S. Patent No. 6,463,813, **2002**, Washington, DC: U.S. Patent and Trademark Office.
13. Wasmer, K.; Nikbin, K. M.; Webster, G. A., Creep crack initiation and growth in thick section steel pipes under internal pressure. *Intl. J. Press. Vessels Pip.*, **2003**, 80(7-8), 489-498.

321   14.   Meis, R. D.; Maragakis, E. M.; Siddharthan, R. Behavior of underground piping joints due to static and
322   dynamic loading. *Technical Report MCEER-03-06,* **2003.**
323   15.   Guo, P. Numerical modeling of pipe–soil interaction under oblique loading. *J. Geotech. Geoenviron.*
324   *Eng.*, **2005**, 131(2), 260-268.
325   16.   Schmitt, C.; Pluvinage, G.; Hadj-Taieb, E.; Akid, R. Water pipeline failure due to water hammer
326   effects. *Fatigue Frac. Eng. Mater. Struct.*, **2006**, 29(12), 1075-1082.
327   17.   Lydell, B.; Riznic, J. OPDE—The international pipe failure data exchange project. *Nucl. Eng. Des.*, **2008**,
328   238(8), 2115-2123.
329   18.   Vazouras, P.; Karamanos, S. A.; Dakoulas, P. Finite element analysis of buried steel pipelines under strike-
330   slip fault displacements. *Soil Dyn. Earthquake Eng.*, **2010,** 30(11), 1361-1376.
331   19.   Wu, G. Y.; Smith, D. J.; Pavier, M. J. Effects of load and displacement controlled bending on plastic
332   collapse of pressurized pipes. *Procedia Mater. Sci.*, **2014**, 3, 1204-1209.
333   20.   Wang, S. Evaluation of underground pipe-structure interface for surface impact load. *Nucl. Des.*, **2017**,
334   317, 59-68.
335   21.   Xu, M.; Shen, D.; Rakitin, B. The longitudinal response of buried large-diameter reinforced concrete
336   pipeline with gasketed bell-and-spigot joints subjected to traffic loading. *Tunnelling Underground Space*
337   *Technol.*, **2017**, 64, 117-132.
338   22.   Ortiz, M.; Pandolfi, A. A variational Cam-clay theory of plasticity. *Comput. Methods Appl. Mech. and*
339   *Eng.*, **2004**, 193(27-29), 2645-2666.
340   23.   Zhang, Y.; Yan, Z. G.; Zhu, H. H.; Ju, J. W. Experimental study on the structural behaviors of jacking
341   prestressed concrete cylinder pipe. *Tunnelling Underground Space Technol.*, **2018**, 73, 60-70.
342   24.   ABAQUS, Theory guide, Release 12.6, ABAQUS, Inc.
343   25.   Hachem, F. E.; Schleiss, A. J. A review of wave celerity in frictionless and axisymmetrical steel-lined
344   pressure tunnels. *J. Fluids Struct.*, **2011**, 27(2), 311-328.
345   26.   Wylie, E. B.; Streeter, V. L.; Suo, L. *Fluid transients in systems*, Vol. 1.; Prentice Hall: Englewood Cliffs, NJ,
346   USA, 1993; p. 464.
347   27.   Joukowsky N. On the Hydraulic Hammer in Water Supply Pipes. Division of Physical Sciences of O.L.E.,
348   University of California, USA, 1897.
349   28.   Halliwell, A. R. Velocity of a water-hammer wave in an elastic pipe. *J. Hydraulics Div.*, **1963**, 89(4), 1-21.